Formation of Methane Hydrate from Polydisperse Ice Powders

Werner F. Kuhs,*,† Doroteya K. Staykova,† and Andrey N. Salamatin‡

GZG Abt. Kristallographie, Georg-August-Universität Göttingen, Göttingen 37077, Germany, and Department of Applied Mathematics, Kazan State University, Kazan 420008, Russia

Received: February 19, 2006; In Final Form: April 5, 2006

Neutron diffraction runs and gas-consumption experiments based on pressure−volume−temperature measurements are conducted to study the kinetics of methane hydrate formation from hydrogenated and deuterated ice powder samples in the temperature range of 245−270 K up to high degrees of transformation. An improved theory of the hydrate growth in a polydisperse ensemble of randomly packed ice spheres is developed to provide a quantitative interpretation of the data in terms of kinetic model parameters. This paper continues the research line of our earlier study which was limited to the monodisperse case and shorter reaction times (Staykova et al., 2003).[1] As before, we distinguish the process of initial hydrate film spreading over the ice particle surface (stage I) and the subsequent hydrate shell growth (stage II) which includes two steps, i.e., an interfacial clathration reaction and the gas and water transport (diffusion) through the hydrate layer surrounding the shrinking ice cores. Although kinetics of hydrate formation at stage II is clearly dominated by the diffusion mechanism which becomes the limiting step at temperatures above 263 K, both steps are shown to be essential at lower temperatures. The permeation coefficient D is estimated as $(1.46 \pm 0.44) \times 10^{-12}$ m^2/h at 263 K with an activation energy $Q_D \approx 52.1$ kJ/mol. This value is close to the energy of breaking hydrogen bonds in ice Ih and suggests that this process is the rate-limiting step in hydrate formation from ice in the slower diffusion-controlled part of the reaction.

1. Introduction

Since their discovery in XIXth century, gas clathrate hydrates, nonstoichiometric inclusion compounds encaging small gas (guest) molecules in a framework of hydrogen bonded water (host) molecules, have been a subject of research with increasing intensity and interest mainly driven by their importance in chemical engineering (see, e.g., Sloan 1998[2]) as well as in geoscience (see, e.g., Max 2003[3] and Max et al. 2006[4]) or planetology (see, e.g., Kargel 2004[5]). They exist as a stable solid phase at high gas pressures and/or low temperatures.[6] Two main crystallographic structures of clathrate hydrates, the von Stackelberg cubic structure I and II, are distinguished both consisting of two types of cavities, small and large cages, that can be occupied by the guest molecules.[2] The phenomena of gas hydrate formation, especially for methane and carbon-dioxide, has grown from pure scientific curiosity to an important factor in the gas industry, economy, and ecology. For instance, the knowledge of formation and decomposition kinetics of CH_4- and CO_2-hydrates would allow for economic storage and transport of these materials in the clathrate form, for future safe extraction of methane from natural hydrate deposits, and would further clarify the role of methane hydrate in the Earth's climate change.[7] The formation from (and the decomposition to) normal hexagonal ice (ice Ih) is of particular importance for permafrost regions and in planetology, in particular for Mars, Titan, and comets. It is also important for the production of synthetic hydrates in the laboratory; a reaction of ice with gases is now widely used for the laboratory formation of gas hydrates based on the work of Kuhs et al.[8] and Stern et al..[9] However, the kinetics of their growth (or dissociation) under these conditions are neither well-known nor properly understood. Using cryo field-emission scanning electron microscopy (FE−SEM), it has been found that, in laboratory and natural conditions, clathrate−hydrate crystals, at least in certain cases, show a characteristic foamlike porous microstructure.[1,10−14] In this context, fundamental investigations of clathrate reactions in well-defined systems are of primary significance. The work on hydrate crystal growth from ice is of particular interest to understand the interaction of gas molecules with disordered (or "quasi-liquid") layers of water molecules at ice and hydrate surfaces, the physics of clathration reactions at ice-hydrate interfaces, and permeation of gas and water molecules through hydrate structures.

This paper, based on the PhD research data by Staykova,[15] is mainly focused on kinetics of methane hydrate formation in long-term gas-consumption (pVT) experiments starting from hydrogenated and deuterated ice Ih powders of known structure, grain size, and specific surface area (SSA) below the quadruple point. It continues a companion study[1] where relatively short-term in-situ neutron diffraction measurements and ex-situ FE−SEM observations of gas hydrate growth on spherical ice particles up to reaction degrees of 10−25% were described and quantitatively interpreted. We address the reader to this publication as well as to Genov et al.[16] for a review of earlier results in this field. As a summary, the principal points will be given in the following sections.

Conventionally, two stages of the hydrate formation process are distinguished. The first relatively rapid stage I is ice-surface coating when an initial, possibly patchy, hydrate film nucleates on and spreads over ice particles. The second one (stage II) is the further growth of the hydrate shell around each shrinking ice core in the sample. In principle, it implies two constituent steps (or sub-stages) of (a) the clathration reaction itself at the

* To whom correspondence should be addressed. E-mail: wkuhs1@gwdg.de. Phone: +49 (0) 551 39-3891. Fax: +49 (0) 551 39-9521.
† Georg-August-Universität, Göttingen.
‡ Kazan State University.

10.1021/jp061060f CCC: $33.50
Published on Web 06/15/2006

inner (ice-hydrate) as well as external (gas-hydrate) interfaces and (b) gas/water mass transport (diffusion) through the hydrate layer. A detailed analysis of SEM images of ice powders during the first hours of hydrate formation at temperatures below 240−250 K allowed us also to suggest that different mechanisms were generally involved in the coating process and, in particular, preferential hydrate formation in cracks and at interparticle contacts may precede the coverage of the regular ice-sphere surface. However, these processes could not be clearly separated, especially at higher temperatures, and a more detailed investigation of the initial hydrate film nucleation and development is needed.

In our first attempt[17] to model the hydrate formation from ice powders we considered a limiting case of a porous and easily permeable hydrate layer growing around the shrinking ice cores. Stage II was assumed to be controlled by the interfacial reaction, and the impact of the gas/water transport mechanisms was neglected. Further studies revealed a considerably more complex situation, including both dense and porous hydrates with pores open on a length scale of a few micrometers only. Thus, the gas/water diffusion through the hydrate shells was explicitly introduced[1] as an important controlling step of the ice-to-hydrate conversion, at least during the final diffusion limited stage III. Due to noticeably lesser density of water in the hydrate phase and its apparent mesoporous microstructure, the growing hydrate layer considerably expands into initial voids of the powder packing, inter-grain contacts substantially develop, and a single-particle diffusion model breaks down. From this point of view, a precise description of the sample microstructural geometry and its evolution with time during the clathration reaction was one of the key problems addressed in Staykova et al..[1] The latter paper and its extension to partly cracked ice particles considered in Genov et al.[16] were confined to systems with monosize particles. The samples prepared by us always have a polydispersed nature, and the initial ice grain ensemble is characterized by a size distribution typically of a log-normal shape. As emphasized in Genov et al.,[16] a monosize approximation is applicable for modeling only in the starting phase of the process (for reaction degrees less than 35−40%), until spatial interactions of the outward-growing hydrate shells become a principal factor which controls the gas flux toward the unreacted ice cores and, hence, the rate of clathration. However, it was shown in Staykova et al.[1] that reaction- or diffusion-limited stages II and/or III cannot be distinguished at such low levels of ice-to-hydrate transformation. Hereinafter, we join these two stages together and consider the interfacial clathration reactions and the diffusive transport mechanisms in a more general way as possible simultaneous contributions of a single (united) stage II. The main emphasis of our present study is (1) to obtain kinetic data from pVT gas consumption measurements in long-duration clathration reactions going to completion and (2) to further develop a theory of the gas-hydrate growth from ice powders accounting for the polydispersity effects which can be applied to these data.

2. Experimental Section

2.1. Experimental Methods and Setups. Neutron diffraction techniques were shown to be the best choice to follow in-situ gas-hydrate formation in a complex sample environment with a time resolution of a few seconds.[18,19] It was employed in Staykova et al.[1] to investigate initial phases of the CH_4- and CO_2-hydrate growth mainly from deuterated ice powders. Here we also used the same equipment as described in Staykova et al.[1] on the high-intensity 2-axis neutron diffractometer D20[20,21] at the Institute Laue-Langevin, Grenoble, France, in two long intermittent runs. However, the limited beam-time allocation at neutron sources and the low accuracy of measurements in hydrogenated samples required a search for alternative approaches in long-term investigations of clathration reactions.

In a closed gas-ice system, hydrate formation kinetics can equally be observed as a continuous pressure drop in the course of the hydrate growth. Thus, gas-consumption (pVT) measurements can be considered as another efficient method to conduct laboratory experiments.[16] The setup used in these experiments is similar to that designed for the neutron diffraction experiments, except for the helium-flow cryostat substituted by the low-temperature bath (Neslab RTE 140 bath/circulator with microprocessor controller); a schematic drawing can be found in Genov et al.[16] The bath temperature is maintained by fluid circulation with an accuracy of ±0.1°C in a temperature range of −40 to 150 °C. The pressure is measured by an electronic pressure sensor (ASHCROFT type KXD) regularly calibrated with accurate Heise mechanical manometers of the CM series. The sensor accuracy is about 0.25% in the range of 0−40 MPa with a linear dependency on temperature from 0 to 50 °C. This sensitivity to the ambient temperature variations can cause additional uncertainty in pressure measurements of about ±0.03% $°C^{-1}$. The RS232 serial communication was established between the sensor electronics and the personal computer to provide continuous data acquisition of the gas pressure. Two identical setups connected to a common gas source were simultaneously engaged in experimental runs on the methane hydrate formation kinetics. They are referred below as Setup 1 and 2.

2.2. Sample Preparation. Well-defined ice Ih powder was used as a starting material in our gas-hydrate formation experiments.[1] It was produced by a shock-freezing method through spraying water into liquid nitrogen. Accidentally produced big grains of >200 μm in diameter were removed by sieving. The remaining material was collected and filled in thin-walled Al cans at an estimated packing density of 60−70%. Before the experimental runs, the starting material was annealed for 3 h at −28 °C in order to eliminate the stacking faults produced by the shock-freezing procedure. The success of the annealing process was checked by diffraction. The Al sample cans were then inserted into the pressure cell.

Ice powder morphology was investigated by FE−SEM.[1,14−16] The obtained pictures showed that most of the ice particles had perfect spherical shapes, except for a few percent of cracked and split spheres. Measurements on different batches sprayed from the same nozzle revealed well reproducible populations of ice particles. Powders of different particle size can be prepared with different nozzles. FE−SEM images were used to determine the size distribution of the ice spheres. Diameters of about 1000 particles were recorded by Image Tool software in each imaged sample. All samples show a similar log-normal size distribution. A typical experimental histogram is depicted in Figure 1a and represents the starting material used in our experimental runs discussed below. It transforms to a symmetric distribution of Gaussian type in logarithmic scale ln*d* (see Figure 1b) with continuous best-fit approximation characterized by a mean value $a = \langle \ln d \rangle \approx 3.8$ with standard deviation $\sigma_a \approx 0.65$. As explained in Appendix A, this corresponds to an actual mean ice sphere radius $\langle r_0 \rangle \approx 26 \pm 1$ μm with relative standard deviation $\sigma_0 \approx 0.7 \pm 0.15$ taking the uncertainties of all imaged samples into account. The main sample-structure and methane−hydrate characteristics are gathered in Table 1.

2.3. Data Collection and Processing. The detailed methodology of in-situ neutron diffraction experiments on gas hydrate

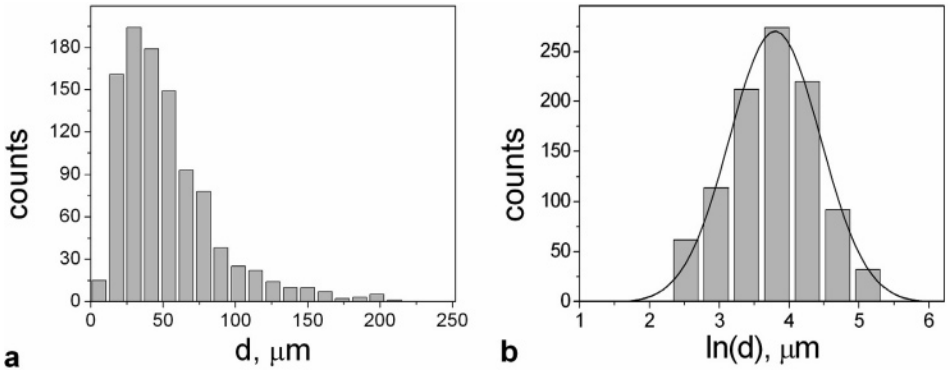

Figure 1. A typical log-normal experimental histogram (a) of initial ice-particle size (diameter) distribution, based on 1006 measurements of deuterated spherical grains imaged by FE−SEM. It converts to the histogram (b) of a normal distribution in a logarithmic scale.

TABLE 1: Characteristics of Ice Samples and Methane Hydrates

parameters and denotations	values
ice samples	
ice density ρ_i, kmol/m^3	51
typical (mean) grain size r_{i0}, μm	26 ± 1
relative standard deviation of grain radii	0.7 ± 0.15
specific surface area S_{i0}, m^2/mol	1.2
macro-porosity ε_{m0}	0.34 ± 0.04
mean coordination number $\bar{Z}_0$	7 ± 1
minimum coordination number Z_{min}	2
coordination number exponent γ	2.1
random density slope of particle distribution C	15.5 ± 1.5
gas hydrates	
water density in hydrate phase ρ_{hw}, kmol/m^3	45
submicron porosity of CH_4-hydrates ε_h	0.15
close-off macro-porosity ε_{mc}	$\sim$0.09

growth from deuterated and hydrogenated ice powders was described earlier in Staykova et al.[1] Series of relatively short-term reaction runs with a duration of 8−23 h had been conducted at different thermodynamic conditions and covered mainly the initial part of the hydrate formation process. We followed the same protocol in the two new intermittent experimental runs which lasted 5−6 days. In both cases, the clathration reaction was started in the He-flow cryostat on the diffractometer and was tracked by the neutron diffraction records for about 20 h. Then the data acquisition was interrupted and the gas-pressure cell (stick) with the sample was moved to a separate low-temperature bath where the reaction was continued out of the beam for a few days. Each stick was placed back into the orange cryostat to measure the current reaction degree two times more: in the middle and at the end of the observation period. The conditions of all experiments discussed below are presented in Table 2.

Prior to each gas-consumption experiment, the pressure lines of both setups were thoroughly checked for being leak proof. Before starting the reaction, each pressure cell was pre-cooled in liquid nitrogen for a few minutes. The high pressure lines were flashed with methane gas, and the ice sample was inserted into the cell under a small stream of methane to ensure a complete filling of the system with the gas. Then the Bridgman seal and the manual valve were closed. The stick was inserted into the bath, already adjusted to a chosen temperature, and left for about 10 min to equilibrate. Then the desired pressure was applied by opening the manual valve for a short time. The reaction began, and the data acquisition of the pressure drop in the closed gas-ice system was launched. The time steps of the data collection typically were 30 s or 1 min during the initial fast stage of the hydrate formation and were increased later to 5, 10, or 15 min when the growth rate slowed. The pressure in the system was adjusted from time to time to maintain it at the chosen level with an accuracy of several percent. The recorded incremental pressure drops were then converted to the corresponding amounts of the consumed gas.

A first series of pVT kinetic runs showed that the pressure measurements were noticeably influenced by daily fluctuations of the ambient air temperature in the laboratory room which were not efficiently suppressed by available air-conditioning facilities. These nonisothermal environmental conditions lead to corresponding changes in the thermodynamic state of the gas passing through the pressure line, especially in the upper part of the stick exposed to the ambient air. Eventually, in all subsequent experiments the environmental temperature was measured near the pressure gauge, and its appropriately scaled variations were subtracted from the original gas-consumption data in order to smooth the kinetic curve.

A special series of hydrate formation experiments was performed simultaneously in both setups I and II at a gas pressure of 6 MPa first with hydrogenated (at 270 K) and then with deuterated (at 263 K) ice powders, and it demonstrated a very good reproducibility between runs on the same material and insignificant differences between deuterated and hydrogenated samples. This point will be additionally addressed below in section 4.

The nonstoichiometry of clathrate solutions[2] does not allow for an accurate estimation of the amount of gas hydrate formed straightforwardly from the gas consumption. Moreover, the dead volume of the setup is not known precisely. Hence, an X-ray diffraction method was used to determine the total reaction degree at the end of each run on recovered samples. To avoid any decomposition of the hydrate upon releasing the pressure, samples were recovered in liquid nitrogen, crushed, and filled in a sample holder also cooled in liquid nitrogen. The measurements were performed at 80 K on a custom-made Philips MRD diffractometer equipped with an APD helium closed-cycle cryostat. The hydrate fractions were obtained with an estimated accuracy of about $\pm$3%. These experimental fractions were used to scale the gas-consumption data.

2.4. FE−SEM Observations. We continued ex-situ scanning electron microscopic studies[1,11,12,14,22] of methane hydrates recovered at different stages of the growth process. A new series of "interrupted" runs at pressure of 6 MPa and temperature of 263 K was performed[15] with eight hydrogenated samples in the laboratory setup used for the pVT measurements; they focused on the initial stage of the hydrate film nucleation and spreading over ice-sphere surface. The reactions were done using identical setups and were stopped after 30 min, 1, 1.5, 2, 3, 4, 8, and 24 h by quenching in liquid nitrogen; the recovered samples were then imaged using FE−SEM[15]. Several hundreds of electron

TABLE 2: Conditions of Experiments and Kinetic Parameters of Methane Hydrate Formation[a]

conditions of experiments							Deduced kinetic parameters				
run	Ice	T, K	p (f), MPa*	p_d (f_d), MPa*	duration, h	final α, %	k_S, 1/h	k_R, kmol/m^{2}h	D, m^2/h	δ_0, μm	$F = D\rho_i/\bar{r}_0 k_R$
neutron diffraction experiments											
1	D_2O	270	6.0(5.19)	2.33(2.20)	135	64.5	0.7	1.1×10^{-4}	1.3×10^{-12}	2.1	0.02
2	D_2O	263	6.0(5.11)	1.84(1.75)	104	41.8	0.2	4.7×10^{-6}	1.3×10^{-12}	1.9	0.39
gas-consumption experiments											
3	D_2O	268	6.0(5.16)	2.19(2.07)	260	80.7	0.4	2.0×10^{-4}	2.1×10^{-12}	4.0	0.015
4	D_2O	263	9.0(7.07)	1.84(1.75)	506	84.6	0.2	2.5×10^{-5}	1.9×10^{-12}	2.9	0.11
5	D_2O	263	3.0(2.77)	1.84(1.75)	506	43.6	0.2	3.4×10^{-6}	8.9×10^{-13}	1.9	0.36
6	D_2O	263	6.0(5.11)	1.84(1.75)	214	67.2	0.2	9.5×10^{-6}	1.4×10^{-12}	1.6	0.20
7	D_2O	263	6.0(5.11)	1.84(1.75)	263	70.7	0.2	5.5×10^{-6}	1.9×10^{-12}	1.5	0.48
8	D_2O	263	6.0(5.11)	1.84(1.75)	263	73.7	0.2	8.0×10^{-6}	1.6×10^{-12}	1.8	0.28
9	H_2O	263	6.0(5.11)	1.84(1.75)	142	63.8	0.2	1.1×10^{-5}	2.1×10^{-12}	2.7	0.27
10	H_2O	258	6.0(5.05)	1.57(1.50)	215	63.2	0.1	7.3×10^{-6}	1.0×10^{-12}	2.5	0.19
11	D_2O	253	6.0(4.99)	1.34(1.29)	340	66.1	0.04	4.5×10^{-6}	7.4×10^{-13}	2.9	0.23
12	H_2O	245	6.0(4.87)	1.03(0.996)	839	43.7	0.025	2.0×10^{-6}	1.5×10^{-13}	5.2	0.11

[a] The fugacities are calculated using the International Thermodynamic Tables of the Fluid State, Vol.5 Methane International Union of Pure and Applied Chemistry, Pergamon Press: Elmsford, NY, 1976

micrographs were examined in total. As before, the CH_4-hydrate phase was identified by the distinct mesoporous structure of its surface.

In agreement with earlier descriptions,[1,16] starting from a well-defined powder of ice spheres, the hydrate phase predominantly nucleates and grows in cracks with simultaneous formation of intergrain hydrate bonds and hydrate patches on the regular ice surface. Subsequently, the initial hydrate film spreads and covers largely all ice particles, leading to a consolidated sample with still distinguishable original structure. The final state of the sample at the end of the coating process looks like a consolidated aggregate of irregularly shaped ice-hydrate particles with scarce open pores visible after breaking the sample. As could be expected from a probabilistic point of view, the described hydrate nucleation and growth picture does not develop uniformly, each time the reaction states differ from grain to grain, different parts of the sample pass through the observed steps of hydrate formation at different rates. Thus, only an upper estimate for the time-scale of the complete coating of all ice grains, not exceeding 10−15 h at the above-mentioned thermodynamic conditions, can be deduced. Eventually, the initial coating of ice surface is followed by inward and outward growth of the hydrate layer.

3. Theoretical Section

3.1. Model of Shrinking Polydisperse Ice Cores. The starting material is described as a random dense packing (ensemble) of polydisperse ice spheres characterized (see Appendix A and Figure 1) by the size distribution function $f_0(r_0)$ of initial radius r_0. As schematically shown in Figure 2, during the gas-hydrate formation process each ice particle transforms to a shrinking ice core of current radius r_i covered by a growing hydrate shell. Each particle has a specific relative environment of surrounding grains, and, in general, its initial size does not determine uniquely its conversion to hydrate. Interaction of a reference ice sphere in the ensemble with neighboring spheres and ambient gas phase can be described only on average. Therefore, radius r_i and other ensemble characteristics should be understood as the respective conditional mean quantities related to all ice-hydrate particles which develop from initial ice grains of the same radius r_0. In this case the number of ice-hydrate particles in each initial size fraction remains constant, and their mean current radius r_i is a monotonically increasing function of r_0. Consequently, the evolving statistical ensemble of particles at any moment t can be

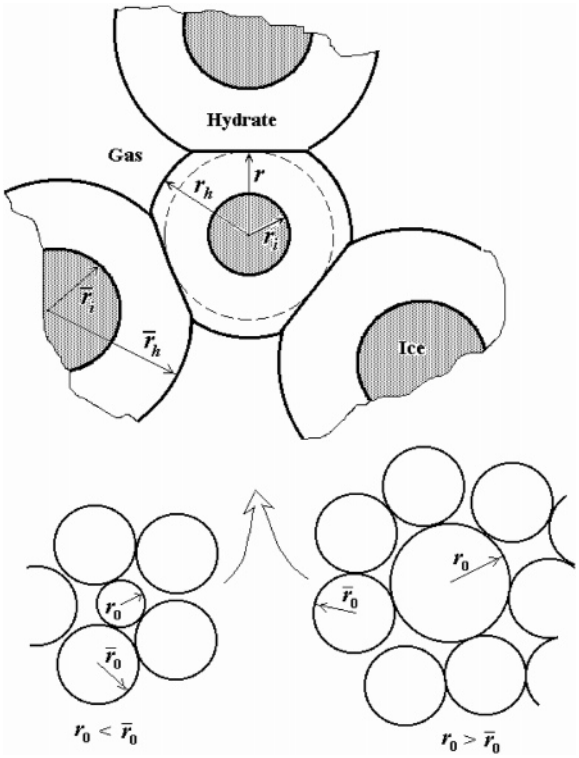

Figure 2. A sketch of the conditionally averaged initial structure of an ice powder sample around a reference particle which is smaller (left) or larger (right) than the "average" particles. The upper part of the drawing illustrates the sample geometry with hydrate shells growing around shrinking ice cores. See explanations in text.

represented by the ice-core size distribution function $f(r_i, t)$ determined by the population balance equation:

$$f(r_i,t) = f_0(r_0)\left[\frac{dr_i(t)}{dr_0}\right]^{-1}, r_i > 0. \quad (1)$$

By definition, the total number fraction of ice grains, which currently are not completely converted to hydrates, is

$$n = \int f(r_i,t)dr_i.$$

Since, in the framework of the above assumption, $r_i = r_i(r_0, t)$, any other ensemble characteristic $\psi(r_i, t)$ can equally be considered as a function of r_0 and t with the ensemble averaged

value $\langle\psi\rangle$ introduced as

$$\langle\psi\rangle = \int \psi(r_0,t) f_0(r_0) dr_0.$$

Accordingly, the initial and current mean-volume radii ($\bar{r}_0$ and $\bar{r}_i$) of ice cores, their specific surface area S_i, and the total reaction degree α are

$$\bar{r}_0 = \langle r_0^3\rangle^{1/3},\ \bar{r}_i = \langle r_i^3\rangle^{1/3},\ S_i = 3\langle r_i^2\rangle/(\rho_i \bar{r}_0^3),\ \alpha = 1 - \bar{r}_i^3/\bar{r}_0^3, \tag{2}$$

where ρ_i is the mole density of ice.

Eventually, the general problem of modeling the gas-hydrate formation from polydisperse powders of randomly packed ice spheres is reduced to a mathematical description of evolution of a single reference grain plunged into the powder medium with conditionally averaged properties of surrounding ice-hydrate particles. The conventional assumption of the self-consistent field theory in statistical physics and mechanics is that the conditionally averaged properties of the system around the reference particle can be identified with the corresponding ensemble means. As a result, we have to consider conversion of a reference ice particle of initial radius r_0 to hydrate in the apparent monodisperse powder with random dense packing of ice spheres of the average radius $\bar{r}_0$, as illustrated by Figure 2. We write the general ice-mass balance equation governing the radius of the shrinking ice core in the reference ice-hydrate particle, after refs 1 and 17, in the following form:

$$\frac{dr_i}{dt} = -\delta_0 \omega_S e^{-\omega_S t} - \frac{\omega_V}{\rho_i}(1 - e^{-\omega_S t}),$$

$$r_{i|t=0} = r_0. \tag{3}$$

As before, δ_0 is the thickness of the ice layer converted to the initial hydrate film of thickness $d_0 = (1 + E)\delta_0$ spreading over the ice-grain surface, where E is the hydrate-volume expansion factor

$$E = \frac{\rho_i}{\rho_{hw}(1 - \varepsilon_h)} - 1$$

expressed via the mole density of water ρ_{hw} and a possibly nonzero meso-porosity ε_h in the clathrate phase. We also designate as ω_S and ω_V the rates of the ice-surface coating and the ice-to-hydrate transformation, respectively. The former quantity can be defined as the fraction of the open (exposed to the ambient gas) ice surface which becomes covered by the initial hydrate film during a unit time period, while the latter one is the number of ice moles transformed to hydrate phase per unit of time on a unit area of ice surface after its coating. Depending on the rate-limiting step of the hydrate formation process during stage II, ω_V describes either the rate of the interfacial clathration reaction or the rate of the gas and water mass transfer through the hydrate shell. Parameter δ_0 is small compared to the initial grain size r_0, whereas the rate of the initial hydrate film formation is assumed to be much higher than that of the hydrate layer growth on the coated surface ($\omega_S \gg \omega_V/\rho_i r_0$), and the ice-core surface area S_i does not noticeably change during stage I.

It should be emphasized that the above assumption of the linear-in-time process of ice grain coating with constant rate ω_S is a certain phenomenological simplification of the real picture, which actually, as discussed in section 2, is a complicated interplay between hydrate nucleation and two-dimensional growth (hydrate film spreading) on ice surface. Sensitivity of both mechanisms to the surface quality in cracks and on regular parts of ice spheres may also be a crucial factor, as considered in refs 15 and 16. In accordance with Genov,[23] it can be expected that a detailed description of the initial stage of gas-hydrate formation will lead to a Johnson−Mehl−Avrami−Kolmogorov nonlinear model[24] combined with the approach based on the convolution integral transform[17]. Nevertheless, here, being concentrated on interpretations of a developed phase of long-term clathration reactions affected by polydispersity of ice powders, we still use eq 3 as an appropriate tool for simulations. A generalized mathematical description of the initial stage I still needs a better experimental basis and will be presented elsewhere.

The driving force of the hydrate formation is the supersaturation of the gas−ice−hydrate system, $\ln(f/f_d)$, expressed via fugacities f and f_d of the gaseous phase related to the imposed and decomposition pressures p and p_d at a given thermostat temperature T. For each stage, this force determines the clathration kinetics and is distributed among different steps of the ice-to-hydrate conversion in proportion to their apparent resistances, namely, k_S^{-1} for the initial hydrate film spreading over the ice surface, k_R^{-1} and k_D^{-1} for the interfacial reaction and gas/water permeation through the hydrate layer, respectively.

Following Staykova et al.,[1] we write

$$\omega_S = k_S \ln\frac{f}{f_d},\ \omega_V = \frac{k_R k_D}{k_R + k_D}\ln\frac{f}{f_d}. \tag{4}$$

The clathration rate constants are assumed to be the Arrhenius-type functions of temperature:

$$k_J = k_J^* \exp\left[\frac{Q_J}{R_g}\left(\frac{1}{T^*} - \frac{1}{T}\right)\right],\quad J = S, R, D, \tag{5}$$

where k_J^* and Q_J are the clathration rate constant at the reference temperature T^* and the activation energy of the J-type step, R_g is the gas constant.

The phenomenological model 1−5 presents a theoretical basis for modeling and detailed analysis of the hydrate formation kinetics in polydisperse powders. For a fixed temperature, k_S and k_R can be considered as tuning parameters. However, the permeation rate constant k_D depends on the sample structure, permeability, and geometrical characteristics of the hydrate layers growing around shrinking ice cores and must be related to r_i and $\bar{r}_i$ (or α) to complete simultaneous equations 1−3.

3.2. Sample Structure Evolution and Permeation Resistance of the Hydrate Layer. As in Staykova et al.,[1] we hold to the general line of the geometrical description of the powder particle growth developed by Arzt[25] for a random dense packing of monosize spheres. The shape of the hydrate layer formed from the reference ice grain (see Figure 2) is represented as a truncated sphere of radius r_h. The ice core shrinks, and its radius r_i decreases because of the inward growth of the hydrate layer. However, because of the lesser density of water in the hydrate phase and its porosity, the excess water molecules must be transported to the outward hydrate surface exposed to the ambient gas, and the hydrate layer simultaneously expands into the open space between the original ice grains. To extend Arzt's[25] approach to the polydisperse powder, hereinafter, the above scenario is also assumed for the "average" ice particles surrounding the reference one. All of them consist of the inner ice core of radius $\bar{r}_i$ occluded in the truncated spherical hydrate shell of external radius $\bar{r}_h$. The existing contact areas between

the reference particle and the neighboring ones increase, and additional contacts are formed as r_h and $\bar{r}_h$ grow. Correspondingly, the specific surface of macro-voids S_m and the macro-porosity of the sample ε_m decrease. Obviously, the evolution of a single reference ice grain of any radius r_0 in the powder must be modeled in interaction with the simultaneous ice-to-hydrate conversion in the surrounding "average" monodisperse medium of randomly packed spheres of radius $\bar{r}_0$. A system of equations which describe the evolution of the polydisperse powder structure in terms of the above characteristics r_i, r_h, and $\bar{r}_i$, $\bar{r}_h$ is formulated below based on Appendix B.

In a random dense packing without particle rearrangement, the current number of contacts (coordination number) Z per a reference grain plunged into the monodisperse powder of average particles can be expressed (see Appendix B) after Arzt[25] as a linear function of the respective hydrate shell radii r_h and $\bar{r}_h$:

$$Z = Z_0 + C\left(\frac{r_h - r_0 + \bar{r}_h - \bar{r}_0}{2\bar{r}_0}\right). \tag{6}$$

Here Z_0 is the initial coordination number of the reference ice grain, and $C \sim 15.5$ is the slope of the random density function in the average monosize particle structure. It is predictable that, in a polydispersed system, Z_0 monotonically increases with the relative size of the particle, and a plausible parametric approximation can be written as

$$Z_0 = Z_{\min} + (\bar{Z}_0 - Z_{\min})(r_0/\bar{r}_0)^{\gamma}, \tag{7}$$

where $\bar{Z}_0 \sim 7$ is the coordination number in the random dense packing of monosize spheres, exponent $\gamma \sim 2$, and minimum coordination number $Z_{\min} \sim 2-3$ are the approximation parameters.

The principal geometric characteristic of the sample structure which determines the interaction of the reference particle with the surrounding medium is the fraction s of the free surface area of the hydrate shell (in units of $4\pi r_h^2$) exposed to the ambient gas. In the polydisperse powder this quantity is related to development of a contact area between two growing spheres (reference and average ones) of different external radii r_h and $\bar{r}_h$. This problem is considered in Appendix B, and the generalized analogue of Arzt's[25] expression extended to polydisperse systems is

$$s = 1 - \frac{\lambda_0 Z_0}{2r_h}(r_h - r_0 + \bar{r}_h - \bar{r}_0) - \frac{\lambda_0 C}{8\bar{r}_0 r_h}(r_h - r_0 + \bar{r}_h - \bar{r}_0)^2, \tag{8}$$

where $\lambda_0 = \bar{r}_0/(r_0 + \bar{r}_0)$. The hydrate layer of the reference particle can grow only on the surface area of $4\pi s r_h^2$ due to the increase in the hydrate volume with respect to the consumed ice volume. The mass balance of water molecules directly relates the rate of the ice core radius decrease governed by eq 3 to the rate of the external hydrate radius increase

$$\frac{dr_h}{dt} = -\frac{E r_i^2}{s r_h^2}\frac{dr_i}{dt}. \tag{9}$$

Correspondingly, for the average grain ($r_0 = \bar{r}_0$, $r_h = \bar{r}_h$) from eqs 8 and 9 we have

$$\frac{d\bar{r}_h}{dt} = -\frac{E \bar{r}_i^2}{\bar{s}\bar{r}_h^2}\frac{d\bar{r}_i}{dt}, \tag{10}$$

where the mean free surface fraction $\bar{s}$ is

$$\bar{s} = 1 - \frac{\bar{Z}_0}{2\bar{r}_h}(\bar{r}_h - \bar{r}_0) - \frac{C}{4\bar{r}_0\bar{r}_h}(\bar{r}_h - \bar{r}_0)^2. \tag{11}$$

Eqs 8−11 determine the evolution of the key geometrical characteristics of the polydisperse ice powder structure r_h and $\bar{r}_h$, which are necessary to close the model 1−4 of the ice-to-hydrate conversion in a powder of polydisperse ice spheres.

The permeation rate constant k_D of the hydrate shell of a given reference particle in eq 4 was found in Staykova et al.[1] as

$$k_D = \frac{\rho_i D}{r_i}\frac{\sqrt{s} r_h r}{\sqrt{s} r_h (r - r_i) + r_i (r_h - r)}, \tag{12}$$

where D is the apparent gas/water mass transfer (permeation) coefficient. The temperature dependence of the latter characteristic is identical to that of k_D in eq 5 with D^* corresponding to the reference temperature T^*. The distance r from the ice core center to an average contact plane (see Figure 2) in eq 12

$$r = r_h\left[1 - \frac{2(1-s)}{Z}\right]$$

determines the spherical boundary of radius r, which divides the hydrate shell into two sublayers from r_i to r and from r to r_h. Relationship 12 is a combination of the permeation (diffusion) resistances of these two layers.

As explained in Appendix C, the initial macro-porosity of the ice sample ϵ_{m0} is directly linked to the structural parameters $\bar{Z}_0$ and C in eqs 6 and 7, the quantity $(1 - \varepsilon_{m0})^{-1}$ being equal to the maximum relative volume of the average ice-hydrate particle with maximum mean particle radius $\bar{r}_h$ attainable at $\bar{s} = 0$. In accordance with definition 2, the current porosity ε_m, and specific surface area of the original macro-pore space between the particles S_m are

$$\varepsilon_m = \varepsilon_{m0} - \alpha(1 - \varepsilon_{m0})E,\ S_m = 3\bar{s}\bar{r}_h^2\langle r_0^2\rangle/(\rho_i \bar{r}_0^5).$$

Due to the gas-hydrate expansion, the permeability of the pore channels formed by the original ice grains in the sample decreases, and the pores get closed at a certain macro-porosity ϵ_{mc}, related to a definite value of the free surface fraction $\bar{s}_c$ of average particles (see Appendix C). Accordingly, in a polydisperse powder, we assume that the gas flow toward a reference grain expires at $s = \bar{s}_c$, and the ice core is switched out of the reaction. As a result, the close-off porosity is preferentially reached near the bigger grains, which become isolated with time before their complete transformation to the hydrate phase.

It should be mentioned that for polydisperse ice powders with log-normal particle-size distributions, a monosize description of the gas-hydrate formation kinetics developed in our companion publication (Staykova et al.[1]) remains valid for the initial part of the clathration reaction and can be directly deduced, as shown in Appendix D, from the general model by averaging eq 3. Ice-particle size should be identified with its mean-volume value $\bar{r}_0$, and $\langle r_i^2\rangle$ in eq 2 should be expressed in accordance with Appendix A via $\bar{r}_i$.

4. Results and Discussion

4.1. Methane−Hydrate Formation Observed in Experiments. The main two long-term neutron diffraction and 10 gas-

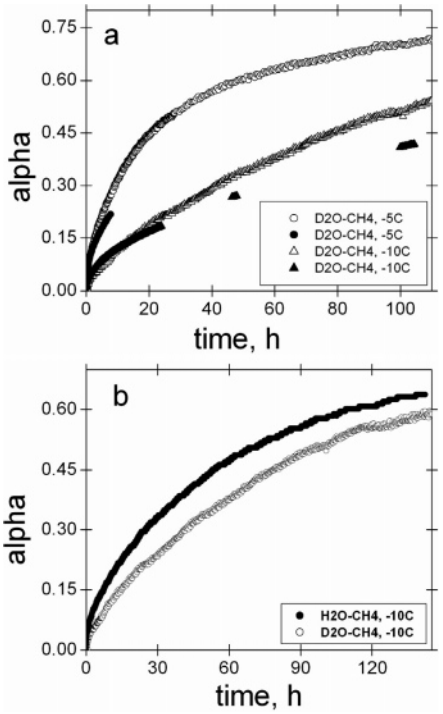

Figure 3. Intercomparison of experimental methods and isotopically different ice powders. (a) Comparison of hydrate formation kinetic curves obtained by diffraction (solid symbols) and pVT (open symbols) methods at pressure 6 MPa for temperatures 268 and 263 K (circles and triangles, respectively). Neutron diffraction measurements are presented by the short-term experiment from Staykova et al.,[1] and intermittent run 2, gas-consumption data correspond to runs 3 and 8 (see Table 2). (b) Methane−hydrate growth from deuterated and hydrogenated ice powders (open and solid circles) in experimental runs 8 and 9, respectively, at 6 MPa and 263 K.

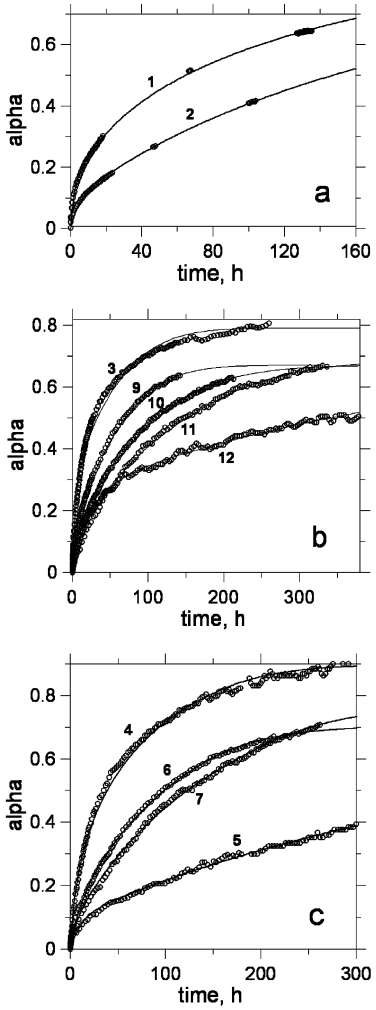

Figure 4. Dependence of methane−hydrate formation kinetics on thermodynamic conditions. (a) Neutron diffraction runs 1 and 2 at 6 MPa for 270 and 263 K, respectively. (b) Gas-consumption experiments 3, 9−12 at 6 MPa for 268, 263, 258, 253, and 245 K, respectively. (c) Gas-consumption kinetic curves at 263 K for different pressures of 9 MPa (run 4), 6 MPa (runs 6 and 7), and 3 MPa (run 5). Experimental data and best-fit simulations are shown by open circles and thin solid lines, respectively. Figures near the curves are the numbers of experimental runs from Table 2.

consumption experiments conducted to investigate kinetics of methane−hydrate growth from H_2O- and D_2O-ice powders at different thermodynamic conditions (7−10 °K below the ice melting point) are listed in Table 2. The intermittent neutron diffraction runs lasted 5−6 days, while the pVT measurements proceeded typically for a few weeks.

We also attempted to perform special series of gas-consumption experiments with hydrogenated ice near the melting point in the temperature range from 268 to 272 K. However, at the very beginning of the reaction, fast ice-grain regrowth in samples at these temperatures led to dramatic decrease in the free ice surface and hindered or, even, suppressed CH_4-hydrate nucleation and further formation. To avoid this problem, we tried to start the reaction at a lower temperature of 266 K for 4 h in order to form an initial hydrate shell around ice spheres and then continued the experimental runs at a desired higher temperature. But even after such preparation clathration reactions in hydrogenated systems for temperatures from 270 to 272°K were slower than at 268°K, and all of them had the rates lower than those recorded in deuterated systems 5−9°K below the D_2O melting point. It is clear that special experimental methods must be developed in future to effectively control the ice-sample structure at high temperatures. Therefore, the data cannot be analyzed in terms of hydrate-formation kinetics and we do not discuss the high-temperature pVT measurements in this paper.

To check the consistency of our kinetic experiments, we compare, in Figure 3a, our results for a deuterated system at gas pressure of 6 MPa and two temperatures of 268 and 263 K obtained by the gas-consumption and neutron diffraction methods, respectively. The respective kinetic curves do not differ considerably although the in-house reactions developed systematically faster. The latter peculiarity can be explained by the fact that in the diffractometer the gas is cooled along the full length of the stick capillary, while in the pVT setup it experiences a strong temperature gradient from the ambient to bath temperature along its way to the sample. In Figure 3b, experimental runs 8 and 9 (see Table 2) with D_2O- and H_2O-ice powders at 6 MPa and 263 K are intercompared. The observed slightly higher rates of hydrate growth from hydrogenated ice could be expected because of the 3.8 K shift between D_2O- and H_2O-ice melting points. This result confirms the earlier conclusion[1] that the isotopic difference plays a minor role in CH_4-hydrate formation kinetics, at least at temperatures well below the melting point.

The long-term diffraction runs 1 and 2 with deuterated systems and gas-consumption experiments 3, 9−12 with deuterated and hydrogenated systems at the basic pressure of 6 MPa are presented in Figure 4a,b, and they illustrate dependence of the methane hydrate formation kinetics on temperature in the range from 245 to 270 K. Obviously, this thermodynamic parameter is the principal factor controlling the clathration

process. Methane hydrate growth at a fixed temperature of 263 K and different gas pressures of 3, 6, and 9 MPa (runs 4−7) in deuterated systems in Figure 4c evidently shows a significant influence of the respective increase in the driving force, $\ln(f/f_d) = 0.46$, 1.07, and 1.40, on the hydrate formation rates. Direct comparison of the kinetic curves likely points out a nonlinear overall dependence of the hydrate growth on the gas-ice system supersaturation. At the same time, despite a good reproducibility of the reaction degree measurements within ±5% deviation (see two limiting kinetic curves 6 and 7 obtained at 6 MPa in Figure 4c), the latter uncertainty can substantially change the estimates of the clathration rates, especially in the final slow stage of hydrate formation controlled by diffusion and sample porosity. Different sensitivity of the hydrate-growth kinetics to excess fugacity at different temperatures was earlier observed in Staykova et al.[1] Hence, additional studies are needed to reliably resolve the influence of the driving force. Hereinafter, to be consistent with our previous works (Staykova et al.[1] and Genov et al.[16]) we assume the linear equation 4. This interferes little with our interpretations of the temperature impact on the hydrate formation kinetics in experimental runs conducted at the fixed pressure.

Long-term gas-consumption kinetic runs, especially at higher temperatures in Figure 4b and c, evidently reveal different limiting levels of the reaction degree at completion of the hydrate growth. It is well-known from snow densification studies (e.g., Martinerie et al.[26] and Lipenkov et al.[27]) that pores in the "natural ice powder" become closed at porosity $\varepsilon_{mc} \sim 0.09$. We assume that this estimate could equally be valid for the random packing of growing ice-hydrate spheres. Then lower reaction degrees at the end of ice-to-hydrate transformation would be observed in ice powder samples with higher initial densities (lower porosities).

4.2. Model Constraining and Data Interpretation. The theory described in section 3 was applied to interpret the diffraction and gas-consumption data presented in Figure 4. An interactive computer program was developed to perform all necessary simulations. A least-squares procedure under user control was performed to iteratively fit the model to the reaction degree measurements. The same approach had been successfully employed in Staykova et al.[1] and Genov et al.[16]. All previous and new preliminary simulations confirmed that certain parts of the kinetic curves were selectively sensitive to the main tuning parameters δ_0, k_R, and D. Experimental estimates for the coating rate constant k_S in eq 4 were derived from our SEM images in interrupted kinetic runs at different temperatures.[1,15,16] Special computational tests showed that most of the conducted gas-consumption experiments were sufficiently long and approached the completion level of the ice-to-hydrate transformation. Thus, assuming that the pore closure in the samples occurs at a fixed porosity $\varepsilon_{mc} \approx 0.09$, we were also able to estimate feasible variations of microstructural parameters $\bar{Z}_0$ and C in eqs 6 and 7 as well as predict (see Appendix C) corresponding changes in the initial sample porosity ε_{m0}, which appeared to be in full agreement with our expectation. All the results of the model constraining are presented in Tables 1 and 2; the best-fit simulated kinetic curves are shown by thin solid lines in Figure 4. Apparently, low-porosity samples with $\varepsilon_{m0} \approx 30\%$ ($\bar{Z}_0 \approx 8$, $C \approx 17$) were used in kinetic runs 6−11 while runs 3 and 4 were conducted in more porous ice powder structures with ε_{m0} up to 38% ($\bar{Z}_0 \approx 6$, $C \approx 14$).

Different peculiarities of the hydrate formation process in polydisperse ice powders revealed in our computational experiments are demonstrated in Figure 5 for typical gas-consumption

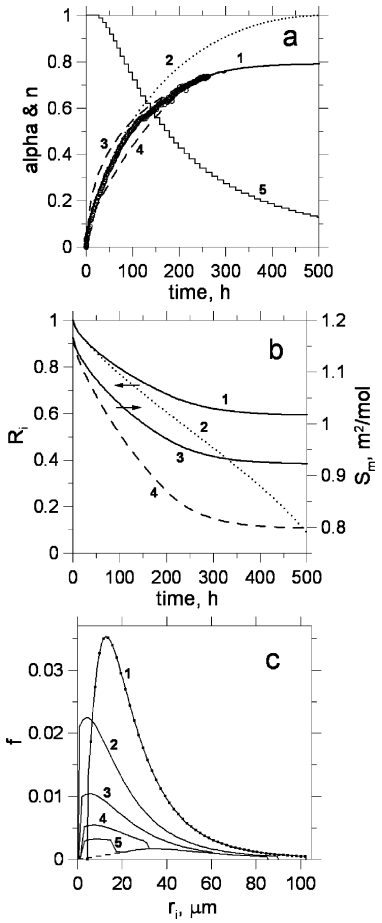

Figure 5. Modeled characteristics of methane hydrate growth from polydisperse ice powder (typical gas-consumption experimental run 8, see Table 2). (a) Reaction degree measurements (open circles) fitted by the simulated hydrate formation kinetic curve 1 and ice-core number fraction (curve 5). Curves 2, 3, and 4 correspond to monosize ice powder approximation, diffusion- and reaction-limited kinetics, respectively. (b) Mean relative ice-core radius decrease in polydisperse (curve 1) and monosize (curve 2) ice powder; changes in specific surface area of all macro-pores (curve 3) and hydrate shells still containing ice cores (curve 4). (c) Ice-core size distributions: initial (curve 1 with particle size fractions shown by dots) and after 125, 250, 375, and 500 h (curves 2−5, respectively).

kinetic run 8 performed at the basic thermodynamic conditions of 6 MPa and 263 K. These measurements fall between analogous runs 6 and 7 shown in Figure 4c. The simulated curve 1 in Figure 5a presents the best fit to the data and corresponds to initial ice powder porosity of about 33% at the mean coordination number $\bar{Z}_0 = 7$ and the random-density-function slope $C = 15.5$ in eqs 6 and 7.

As discussed in refs 1 and 14, the thickness δ_0 of the ice layer converted to the initial hydrate film controls the steep rise of the reaction degree in the very beginning of the gas-hydrate growth, during stage I, which is estimated to be not longer than 10−15 h in the case of run 8 at $k_S = 0.2$ h^{-1}. Typical values $\delta_0 \sim 2-3$ μm are obtained in our simulations. Specific surface area measurements of methane hydrate[22] indicate that the submicrometer pores observed in our SEM work are predominantly closed with a mean open pore length of a few micrometers, remarkably similar to the estimated values of δ_0. From our observation we have to expect that for thicknesses larger than a few μm some bulk diffusion is necessary for the transfer from or to the reaction front in an ice grain; this expectation is supported by our model fits.

In accordance with eq 4, the next stage II of the hydrate formation is determined, in general, by the two steps (sub-stages) of (1) the clathration reaction itself at ice-hydrate and gas-hydrate interfaces and (2) the diffusive mass transfer of gas and water molecules through hydrate shells surrounding shrinking ice cores. In limiting scenarios, the hydrate-layer growth rate ω_V is controlled only by one of these steps, depending on whether the dimensionless factor[1]

$$F = \frac{D\rho_i}{\bar{r}_0 k_R}$$

is large or small for reaction- or diffusion-limited cases, respectively. The best-fit value $F = 0.28$ in the experimental run 8 shows that the gas/water transport dominates as a hydrate-formation mechanism, although the interfacial reaction may also play an important role. Curves 3 and 4 in Figure 5a illustrate the sensitivity of the hydrate growth process to the ratio of the principal kinetic parameters k_R and D. Standard deviations between measurements and simulations become four times higher when F tends to 0 or ∞. This seems to be true for the whole low-temperature range 245−263 K with typical estimates $F \sim 0.1-0.4$ in Table 2. However, as pointed out in previous model investigations,[1] the reaction degree level of 0.4−0.5 achieved in experimental runs 5 and 12 is too low to reliably distinguish between the reaction and diffusion impacts. Therefore, the best fits in these cases were constrained to the above range of F-factor. At higher temperatures 268−270 K (runs 1 and 3) close to ice melting point, the ratio F becomes small, hydrate formation is limited by diffusion, and only lower estimates for reaction rate constant k_R can be actually inferred.

A crucial difference between gas-hydrate growth from polydisperse and monosize ice powders (compare curves 1 and 2 in Figure 5a) must be emphasized in the developed phase of ice-to-hydrate conversion at reaction degree α exceeding 35−40%. This results from a much slower transformation of bigger ice spheres into hydrates in comparison with the smaller ones. Additionally, in accordance with theoretical concepts presented in section 3, the bigger particles in a polydisperse ensemble are characterized by large coordination numbers Z_0 (see eq 7) and, with high degree of probability, are surrounded by many ice grains of smaller size. The latter ones quickly transform to hydrates, and the pores near the biggest ice cores become closed. As a result, the large-size fraction of the ice powder is eventually switched out of the clathration reaction. Accordingly, the decreasing number fraction of nonreacted ice cores n plotted as curve 5 in Figure 5a does not tend to zero. The steps on the curve reflect the disappearance of certain ice-particle size fractions at their complete conversion to clathrates. On the contrary, in monosize systems all ice spheres uniformly, on average, transform to gas hydrates, and the close-off porosity level may not be reached at all, depending on the initial sample density and the hydrate-volume expansion factor E. This conclusion becomes even more obvious if the mean relative ice-core radii $\bar{R}_i = \bar{r}_i/\bar{r}_0$ in polydisperse and monosize ice powders are compared in Figure 5b (curves 1 and 2, respectively). Specific surface area ("SSA"; curve 4) of hydrate shells still containing unreacted ice cores in the polydisperse sample is systematically less than the total SSA of macro-pores S_m (curve 3). It is also clear that the hydrate formation kinetics in polydisperse ice powders must be sensitive to the relative standard deviation of the particle size distribution σ_0, which at the same time is a measure of the ensemble deviation from the monosize limit. Computational experiments show that possible $\pm 10-15\%$ variations of σ_0 lead to comparable changes in inferable kinetic parameters, eventually increasing their uncertainty.

The modeled evolution of the ice-core size distribution function in the course of the clathration reaction is depicted in Figure 5c. In the beginning, all ice cores shrink without any noticeable decrease in number (see curve 5 in Figure 5a), and the initial size distribution (curve 1) in Figure 5c simply shifts to the left. Gradually more and more ice grains are completely transformed to hydrates, and the smaller-size fractions of ice cores are cut off (see curves 2−5 in Figure 5c). At the same time an increasing number of larger ice grains becomes isolated, and the right-hand part of the ice-core distribution function does not change with time any more, revealing the limiting distribution of unreacted ice cores at the completion of the reaction.

4.3. Kinetic Parameters of Methane−Hydrate Formation. The principal kinetic parameters, reaction rate constant k_R, and permeation (mass-transfer) coefficient D, inferred from the neutron diffraction and gas-consumption data in our computational experiments are gathered in Table 2. They show an obvious tendency to increase with temperature. Hence, the methane−hydrate formation process appears to be temperature activated and we assume the Arrhenius behavior described by eq 5. It has already been mentioned in section 3 that we need a more sophisticated model to interpret the initial stage of gas-hydrate nucleation and two-dimensional hydrate film spreading over ice sphere surface. Therefore, only plots of k_R and D against reciprocal temperatures are presented in Figures 6a and b. Only mean values of the two kinetic parameters obtained at 263 K for different pressures in experimental runs 2 and 4−8 with deuterated samples are shown together with corresponding error bars. The respective activation energies of the least-squares Arrhenius approximations are calculated to be $Q_R \approx 92.8$ kJ/mol and $Q_D \approx 52.1$ kJ/mol.

The rather high uncertainty level of the inferred reaction rate constant k_R and corresponding activation energy Q_R in Figure 6b should be emphasized. This most likely is a consequence of the observed domination of the diffusion mechanism at $F < 0.2-0.35$ additionally enhanced by anomalous development of quasi-liquid layers on ice-hydrate and gas-hydrate interfaces at temperatures above 263 K. Approximately two times lower activation energies of interfacial reaction were found in Staykova et al.[1] and Genov et al.[16] both for CH_4- and CO_2-hydrate formation. Only initial parts of kinetic curves, also dominated by gas/water diffusion through hydrate shells, were examined in these papers. These data did not allow accurate resolving of the reaction impact, diminishing its significance. Although still being uncertain, much higher activation energy Q_R found in our new long-term experimental runs reflects the onset of the diffusion-limited regime of the hydrate growth at temperatures close to ice melting point.

The diffusion activation energy for CH_4-hydrate formation is estimated with an uncertainty not higher than $\pm 20\%$. Being comparable with our previous preliminary results,[1] it is close to Wang's et al. estimate[19] of 14.7 kcal/mol (61.3 kJ/mol) and practically coincides with $Q_D \approx 54.6$ kJ/mol deduced in Genov et al.[16] for CO_2-hydrate growth from ice powders. Thus, it appears that the rate-limiting step in the diffusion-controlled regime is independent of the nature of the gas molecules with CO_2 and CH_4 being quite different in size as well as in molecular interaction with water molecules. This suggests that the rate-limiting step is related to the water molecules' mobility. It is interesting to note that the energy needed to break a hydrogen bond in ice is 12.7 kcal/mol (53.2 kJ/mol)[28] which is very close

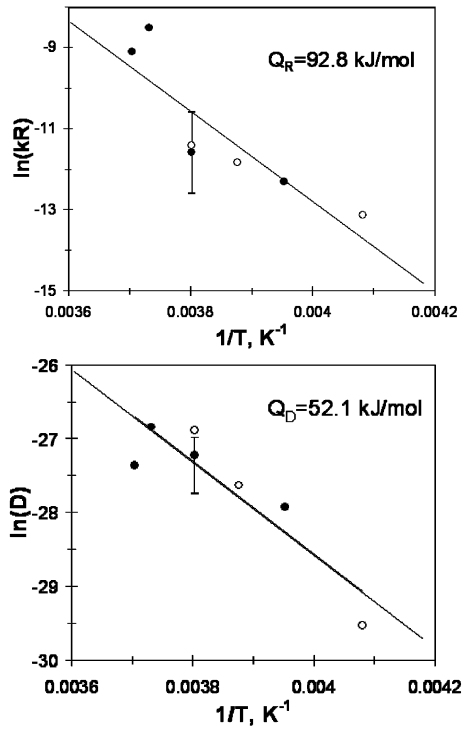

Figure 6. Arrhenius plots of reaction rate constant k_R (a) and permeation coefficient D (b) versus reciprocal temperature. Solid and open circles are the best fit values inferred from the experimental runs with deuterated and hydrogenated samples, respectively (see Table 2). Error bars show the variation of parameters obtained at 263 K for different pressures.

to the experimental values found in the diffusion-controlled stage of hydrate formation. Similar respective activation energies 48 and 54 kJ/mol for N_2- and O_2-diffusion in ice were predicted in a review paper on air hydrates in (ant)arctic ice cores.[29] This may additionally suggest that the gas molecules' diffusive transport properties in polycrystalline ice are related to the breaking of hydrogen bonds in ice. Using eq 5 and the above estimate of Q_D, one can easily reduce the best-fit values of D from Table 2 inferred at different temperatures to a certain reference temperature, which in our case can be taken as $T^* = 263$ K. This procedure yields $D^* = (1.46 \pm 0.44)\cdot 10^{-12}$ m^2/h.

5. Conclusion

Intermittent neutron-diffraction runs and long-term gas-consumption experiments based on pVT measurements are conducted to study kinetics of methane hydrate formation from ice-Ih powders in hydrogenated and deuterated samples. We distinguish a relatively short initial stage I of hydrate film formation on the ice surface and the subsequent stage II which generally includes two steps (sub-stages) presented by the clathration reaction at the ice-hydrate and gas-hydrate interfaces and by the gas and water transport (diffusion) through the hydrate shells surrounding shrinking ice cores.

An improved model for the hydrate growth in a polydisperse ensemble of randomly packed ice spheres is developed to provide a quantitative interpretation of the data in terms of kinetic model parameters. The difference in size of spherical ice particles in polydisperse samples results in different rates of their conversion to hydrates and the larger-size fraction becomes currently isolated and switched out of the reaction. This additionally slows down the ice-to-hydrate conversion and stops the hydrate growth in the sample before the complete transformation is achieved. Our model fits then suggest that for a full transformation of ice into hydrate a small spread of initial ice particle sizes is beneficial; observations for incomplete reactions may then be rationalized when ice particles distinctly larger than average were present initially. Based on the model, an interactive computer system is implemented to facilitate simulations and laboratory data interpretation.

It is shown that stage II, being dominated by the diffusive gas/water transport through the growing hydrate layer, still may be noticeably influenced by the interfacial clathration reaction. The principal kinetic parameters, reaction rate constant k_R, and permeation (mass-transfer) coefficient D, inferred from the neutron diffraction and gas-consumption data in our computational experiments are gathered in Table 2. The respective activation energies of the least-squares Arrhenius approximations are calculated to be $Q_R \approx 92.8$ kJ/mol and $Q_D \approx 52.1$ kJ/mol. The rather high uncertainty level of the inferred reaction rate constant k_R and corresponding activation energy Q_R should be emphasized. This most likely is a consequence of the observed domination of the diffusion mechanism additionally enhanced by an anomalous development of disordered or quasi-liquid layers on ice-hydrate and gas-hydrate interfaces at temperatures above 263 K. The obtained activation energy of the rate-limiting diffusion process is in good agreement with our earlier result.[1] It is close to Wang's et al. estimate[19] of 14.7 kcal/mol (61.3 kJ/mol) and practically coincides with $Q_D \approx 54.6$ kJ/mol deduced in Genov et al.[16] for CO_2-hydrate growth from ice powders. All activation energies are close to the activation energy of breaking hydrogen bonds in ice Ih[28] suggesting that the rate-limiting step in all processes is the rearrangement of water molecules.

Acknowledgment. We are grateful to Thomas Hansen, Louis Melesi, and Jean-Luc Laborier (Institute Laue-Langevin, Grenoble) for their help in performing the high pressure neutron equipment. We also thank Alice Klapproth, Stephan Klapp, and Georgi Genov (GZG, University of Göttingen) for discussions and help during sample preparation and data analysis. We especially acknowledge the work done by Evgeny Goreshnik (GZG), who performed the X-ray measurements. This research was supported by the DFG grant Ku920/9 and through the BMBF Project 03G0553A and 03G0605B within the German research initiative GEOTECHNOLOGIEN; the paper is its publication no. GEOTECH-222.

Appendix A

Ice Sphere Ensemble. We assume that the experimental grain-size fractional histogram of the starting material (ice powder) can be approximated by the log-normal distribution:

$$\varphi_0(y) = \frac{1}{y\sigma_a\sqrt{2\pi}} \exp\left[-\frac{(\ln y - a)^2}{2\sigma_a^{\,2}}\right]$$

where initial ice sphere size y can be understood either as the particle diameter d or radius r_0. Statistical parameters of the distribution $a = \langle \ln y \rangle$ and $\sigma_a^2 = \langle (\ln y - a)^2 \rangle$ are the mathematical expectation (mean) and variance of the random variable ln$y$, respectively. Correspondingly, mathematical expectation $\langle y \rangle$ and variance σ_y^2 of the sphere size y in the ice powder are

$$\langle y \rangle = \exp(a + 0.5\sigma_a^{\,2}),\ \sigma_y^{\,2} = \langle y \rangle^2 [\exp(\sigma_a^{\,2}) - 1]$$

and $\sigma_0 = \sigma_y/\langle y \rangle$ is the relative standard deviation.

Based on general properties of the log-normal distribution, for any exponent ν we have

$$\langle y^{\nu}\rangle = (\bar{y})^{\nu}\exp[0.5\nu(\nu - 3)\sigma_a{}^2], \bar{y} = \langle y^3\rangle^{1/3}.$$

The latter formula can be used to express the moments $\langle y^{\nu}\rangle$ via the mean-volume value $\bar{y}$.

Actually in experiments we deal with a truncated form of the above presentation, which is nonzero only within a certain finite interval of ln$y$. Hereinafter in simulations the 2.5%-accuracy range of ln$y$-variation for the log-normal law is fixed with the limits $a \pm 2.25\sigma_a$. In terms of ice sphere radius r_0, this means that the initial density of the grain number distribution by the grain size is taken as

$$f_0(r_0) = \begin{cases} 1.025\varphi_0(r_0), & r_0 \in [r_{min}, r_{max}]; \\ 0, & r_0 \notin [r_{min}, r_{max}]. \end{cases}$$

$$r_{min} = \exp(a - 2.25\sigma_a), r_{max} = \exp(a + 2.25\sigma_a).$$

Appendix B

Volume Interaction of Two Contacting Spheres Growing in a Polydisperse Powder. Let us first consider the growth of two fixed spheres with radii r_{10} and r_{20} at the moment of their touching, as shown in Figure 7. The distance between their centers remains constant. The radius of the developing contact area r' can be equally expressed via the current radius of one of the spheres r_1 (or r_2) and the distance r_1' (or r_2') from its center to the interface. Hence, we have

$$r_1' + r_2' = r_{10} + r_{20}$$

$$(r')^2 = r_1^2 - (r_1')^2 = r_2^2 - (r_2')^2. \qquad \text{(B1)}$$

For relatively small increments $\delta r_1 = r_1 - r_{10}$ and $\delta r_2 = r_2 - r_{20}$ these equations directly yield

$$r'_1 = r_{10} - \frac{r_{20}\delta r_2 - r_{10}\delta r_1}{r_{10} + r_{20}}, r'_2 = r_{20} + \frac{r_{20}\delta r_2 - r_{10}\delta r_1}{r_{10} + r_{20}}. \qquad \text{(B2)}$$

Consequently, the heights $h_1 = r_1 - r_1'$ and $h_2 = r_2 - r_2'$ of the spherical caps cut from the grown spheres by the contact plain (see Figure 7) are

$$h_1 = \frac{r_{20}(\delta r_1 + \delta r_2)}{r_{10} + r_{20}}, h_2 = \frac{r_{10}(\delta r_1 + \delta r_2)}{r_{10} + r_{20}}. \qquad \text{(B3)}$$

Eq B2 and B3 show that the contact plain between the two growing spheres of different radii does not retain its initial position at the touching point, and moves as the sphere radii increase.

Without any loss of generality, let us assume that sphere 1 in Figure 7 represents one particle from the averaged ambient medium ($r_1 = \bar{r}_h$), and sphere 2 is the reference particle ($r_2 = r_h$). Then, in accordance with Arzt,[25] we introduce the slope C of the radial distribution function in a random dense packing of monosize spheres around the reference particle and write a linear dependence (6) for the coordination number Z of the reference particle on the sum of the increments of both radii $r_h - r_0 + \bar{r}_h - \bar{r}_0$ normalized by $2\bar{r}_0$.

For each new act of touching between the reference sphere and one of the surrounding average spheres during their growth, the ratio of their current radii (r_{20} and r_{10} in Figure 7) can be approximately expressed via the initial radii values

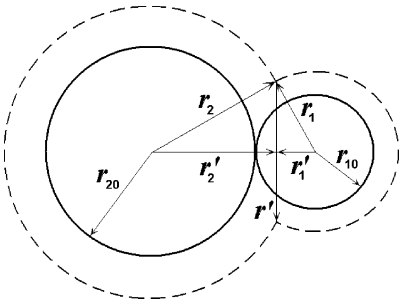

Figure 7. Schematic drawing of volume interaction of two growing spherical particles of different initial radii with fixed centers. See explanations in text.

$$\lambda_0 = \frac{r_{10}}{r_{20} + r_{10}} \approx \frac{\bar{r}_0}{r_0 + \bar{r}_0},$$

Consequently, from eq 6 and B3 the number Z' of spherical caps with heights from $h_0 = \lambda_0(r_h - r_0 + \bar{r}_h - \bar{r}_0)$ to h cut from the reference particle by the contact plains is

$$Z' = Z_0 + C'(h_0 - h), C' = C/(2\bar{r}_0\lambda_0).$$

Finally, following Arzt,[25] we calculate the total (excess) volume of the cutoff caps on the truncated sphere representing the reference particle as

$$v'_{ex} = \frac{\pi Z_0}{3}h_0{}^2(2r_h + r'_h) + \frac{\pi C'}{12}h_0{}^3(3r_h + r'_h),$$

where $r_h' = r_h - h_0$ is the analogue of r_2' in eqs B1 and B2.

Combining the two latter equations results in the volume of the reference particle (ice core + hydrate shell) represented, as shown in Figure 2, in the form of the truncated sphere

$$v'_h = \frac{4\pi}{3}r_h{}^3 - \frac{\pi Z_0}{3}(r_h - r'_h)^2(2r_h + r'_h) - \frac{\pi C}{24\bar{r}_0\lambda_0}(r_h - r'_h)^3(3r_h + r'_h).$$

Actually, this volume does not exactly consists of hydrate produced from the initial ice sphere of the radius r_0 and may lose or acquire some amount of the hydrate due to the difference in grain size and the movement of the contact plains. However, the free surface of the particle s_h' can be correctly calculated by differentiation of v_h' with respect to r_h at constant r_h':

$$s'_h = 4\pi r_h{}^2 - 2\pi Z_0 r_h(r_h - r'_h) - \frac{\pi C}{2\bar{r}_0\lambda_0}r_h(r_h - r'_h)^2.$$

Subsequent dividing by $4\pi r_h{}^2$and substitution of r_h' and h_0 lead to eq 8.

Appendix C

Initial and Close-off Porosities of the Sample. Eq 10 after substitution of eq 11 can be explicitly integrated to relate the normalized volume $\bar{V}_h$ of an average particle measured in units of $(4/3)\pi\bar{r}_0{}^3$ (or its external normalized radius $\bar{R}_h = \bar{r}_h/\bar{r}_0$) to the reaction degree α.

$$\bar{V}_h(\bar{R}_h) \equiv \bar{R}_h{}^3 - \frac{\bar{Z}_0}{4}(\bar{R}_h - 1)^2(2\bar{R}_h + 1) - \frac{C}{16}(\bar{R}_h - 1)^3(3\bar{R}_h + 1) = 1 + \alpha E, \quad \text{(C1)}$$

Obviously, $\bar{V}_h$ reaches its maximum, when $\bar{s} = 0$ in eq 11, and all macro-voids between original ice grains are filled, that is at

$$\bar{R}_h = \bar{R}_{\max} = 1 + \frac{2 - \bar{Z}_0 + \sqrt{(\bar{Z}_0 - 2)^2 + 4C}}{C}.$$

As a result, the current ε_m and initial ε_{m0} porosities of the sample are

$$\varepsilon_m = \frac{\bar{V}_h(\bar{R}_{\max}) - \bar{V}_h(\bar{R}_h)}{\bar{V}_h(\bar{R}_{\max})}, \; \varepsilon_{m0} = \frac{\bar{V}_h(\bar{R}_{\max}) - 1}{\bar{V}_h(\bar{R}_{\max})}$$

and eq C1 allows explicit expression of ε_m via ε_{m0} and α.

Correspondingly, at the close-off porosity ε_{mc} the normalized average radius of the ice-hydrate particle $\bar{R}_{hc}$ is determined by the equation

$$\bar{V}_h(\bar{R}_{hc}) = \frac{1 - \varepsilon_{mc}}{1 - \varepsilon_{m0}}.$$

Finally, the free surface fraction at the pore close-off is calculated (see eq 11) as

$$\bar{s}_c = 1 - \frac{\bar{Z}_0}{2\bar{R}_{hc}}(\bar{R}_{hc} - 1) - \frac{C}{4\bar{R}_{hc}}(\bar{R}_{hc} - 1)^2.$$

Appendix D

Averaged Monosize Approximation for the Earlier Phase of Hydrate Formation. We can now use the basic eq 3 to derive the averaged mass balance relation governing the gas hydrate growth from the powder directly in terms of the reaction degree α. This can be done explicitly only for the beginning of the clathration process when the number of ice cores does not change i.e., until only few smaller ice grains have been completely converted to hydrates and/or bigger ice grains have not been isolated, yet.

For relatively small reaction degree α, hydrate shell geometry and size (curvature) are not important in eqs 4 and 12, $s \approx 1$, $r_i \approx r_h \approx r \approx r_0$, and the hydrate formation rate ω_V is mainly determined by the hydrate layer thickness $r_h - r_i$. Consequently, the right-hand side of eq 3 does not significantly depend on r_0, that is $dr_i/dr_0 \approx 1$ in eq 1. As a result, the ice-core size distribution function retains its initial log-normal shape and is simply shifted with time to the left along the r_i-axis. So, multiplication of eq 3 by $r_i^2 f_0(r_0)$ and its integration with respect to r_0 yields the averaged equation of the same structure as the phenomenological one used in the monosize approximation[1]:

$$\frac{d\alpha}{dt} = S_i[\rho_i \delta_0 \omega_S e^{-\omega_S t} + \bar{\omega}_V(1 - e^{-\omega_S t})], \quad \text{(D1)}$$

where α and S_i are determined by eq 2. The averaged hydrate formation rate $\bar{\omega}_V$ is expressed by relations analogous to eqs 4 and 12 via the mean geometrical characteristics of the ice-hydrate particles $\bar{r}_i$, $\bar{r}_h$, and $\bar{r}$.

Based on the general properties of log-normal distributions described in Appendix A, we have

$$\langle r_i^2 \rangle \approx \frac{\bar{r}_i^2}{1 + \sigma_0{}^2}$$

and express S_i in terms of $\bar{r}_i$ (or α):

$$S_i \approx \frac{3(1 - \alpha)^{2/3}}{\rho_i \bar{r}_0 (1 + \sigma_0{}^2)}.$$

It should be also noted that even for developed diffusion-limited stage of hydrate growth, the diffusion rate constant k_D given by eq 12 is inversely proportional to r_i. The averaging procedure applied to the basic eq 3 after multiplication by r_i^2 would lead to a term $\langle r_i^2 \omega_V \rangle \sim \langle r_i \rangle$. Again, assuming the ice-core size distribution being approximately a log-normal one, we calculate that

$$\langle r_i \rangle \approx \frac{\bar{r}_i}{1 + \sigma_0{}^2}$$

and arrive at eq D1 with the same correction factor $1 + \sigma_0^2$.

References and Notes

(1) Staykova, D. K.; Kuhs, W. F.; Salamatin, A. N.; Hansen, T. Formation of porous gas hydrates from ice powders: Diffraction experiments and multistage model. *J. Phys. Chem. B* **2003**, *107*, 10299−10311.

(2) Sloan, E. D., Jr. *Clathrate Hydrates of Natural Gases*, 2nd ed.; Marcel Dekker Inc.: New York, 1998.

(3) *Natural Gas Hydrate in Oceanic and Permafrost Environments*, 2nd ed.; Max, M. D, Ed.; Kluwer Academic Publishers: London, 2003.

(4) *Economic Geology of Natural Gas Hydrate;* Max, M. D., Johnson, A. H., Dillon, W. P., Eds.; Springer: Dordrecht, The Netherlands, 2006.

(5) Kargel, J. S. *Mars; a warmer, wetter planet;* Springer: Berlin, 2004.

(6) van der Waals, J. H.; Platteeuw, J. C. Clathrate solutions. *Adv. Chem. Phys.* **1959**, *2*(1), 1−57.

(7) Kennett, J. P.; Cannariato, K. G.; Hendy, I. L.; Behl, R. J. *Methane hydrates in Quaternary climate change: The clathrate gun hypothesis;* American Geophysical Union: Washington DC, 2002.

(8) Kuhs, W. F.; Dorwarth, R.; Londono, D.; Finney, J. L. In-situ study on composition and structure of Ar-clathrate. In *Physics and Chemistry of Ice;* Maeno N., Hondoh, T., Eds.; Hokkaido University Press: Sapporo, 2002; pp 126−130.

(9) Stern, L.; Kirby, S. H.; Durham, W. B. Peculiarities of methane clathrate hydrate formation and solid-state deformation, including a possible superheating of water ice. *Science* **1996**, *273*, 1843−1848.

(10) Kuhs W. F.; Klapproth, A.; Gotthardt, F.; Techmer, K.; Heinrichs, T. The formation of meso- and macroporous gas hydrates. *Geophys. Res. Lett.* **2000**, *27*(18), 2929−2932.

(11) Klapproth, A. 2002. Ph.D. Thesis, Universität Göttingen. Strukturuntersuchungen an Methan- und Kohlenstoffdioxid-Clathrat-Hydraten.

(12) Klapproth, A.; Goreshnik, E.; Staykova, D.; Klein H.; Kuhs W. F. Structural Studies of Gas Hydrates. *Can. J. Phys.* **2003**, *81*, 503−518.

(13) Staykova, D. K.; Hansen, T.; Salamatin, A. N.; Kuhs, W. F. Kinetic diffraction experiments on the formation of porous gas hydrates. In. *Proceedings of the Fourth International Conference on Gas Hydrates, Yokohama, May 19−23, 2002;* 537−542.

(14) Stern, L. A.; Kirby, S. H.; Circone, S.; Durham, W. B. Scanning electron microscopy investigations of laboratory-grown gas clathrate hydrates formed from melting ice, and comparison to natural hydrates. *Am. Mineral.* **2004**, *89*, 1162−1175.

(15) Staykova, D. K. 2004. Ph.D. Thesis, Universität Göttingen. Kinetic Studies of Methane-Hydrate Formation from Ice Ih.

(16) Genov, G.; Kuhs, W. F.; Staykova, D. K.; Goreshnik, E; Salamatin, A. N. Experimental studies on the formation of porous gas hydrates. *Am. Mineral.* **2004**, *89*, 1228−1239.

(17) Salamatin, A. N.; Kuhs W. F. In Formation of porous gas hydrates. *Proceedings of the Fourth International Conference on Gas Hydrates, Yokohama, May 19−23, 2002, Yokohama; 766−770*.

(18) Henning, R. W.; Schultz, A. J.; Thien, V; Halpern, Y. Neutron diffraction sudies of CO_2 clathrate hydrate: formation from deuterated ice. *J. Phys. Chem. A* **2000**, *104*, 5066−5071.

(19) Wang, X.; Schultz A. J.; Halpern Y. Kinetics of methane hydrate formation from polycrystalline deuterated ice. *J. Phys. Chem. A* **2002**, *106*, 7304−7309.

(20) Convert, P.; Hansen, T.; Oed, A.; Torregrossa, J. D20 high flux two axis neutron diffractometer. *ICNS'97 Proc., Phys. B* **1998**, *241*−*243*, 195−197.

(21) Convert, P.; Hansen, T.; Torregrossa, J. The high-intensity two axis neutron diffractometer D20 − first results. *Proc. EPDIC6 Mater. Sci. Forum* (Trans. Technology Publications) **1999**, *321*−*324*, 314−319.

(22) Kuhs, W. F.; Genov G. Y.; Goreshnik E.; Zeller A.; Techmer K.; Bohrmann G. The impact of porous microstructures of gas hydrates on their macroscopic properties. *Intern. J. Offshore Polar Eng.* **2004**, *14(4), 305*−*309*.

(23) Genov, G. 2005. Ph.D. Thesis, Universität Göttingen. Physical processes of the CO_2 hydrate formation and decomposition at conditions relevant to Mars.

(24) Humphreys F. J.; Hatherly M. *Recrystallization and Related Annealing Phenomena*, 2-d impression; Pergamon Press: Elsevier: Oxford, 2002.

(25) Arzt, E. The influence of an increasing particle coordination on the densification of spherical powders. *Acta Metall.* **1982**, *30*, 1883−1890.

(26) Martinerie, P.; Lipenkov V. Ya.; Raynaud D.; Chappellaz J.; Barkov N. I.; Lorius C. Air content paleo record in the Vostok ice core (Antarctica): a mixed record of climatic and glaciological parameters. *J. Geophys. Res.* **1994**, *99*(D5), 10 565−10 576.

(27) Lipenkov, V. Ya.; Ryskin O. A.; Barkov N. I. O svyazi mezhdu kolichestvom vozdushnyh vklyucheniy vo l'du i usloviyami l'doobrazovaniya [Relationship of number of air inclusions in ice with ice formation conditions]. *Mater. Glyatsiol. Issled.* **1999**, *86*, 75−91.

(28) Itagaki, K. Self-diffusion in single-crystal ice. *J. Phys. Soc. Jpn.* **1967**, *22*, 427−431.

(29) Ikeda, T.; Salamatin, A. N.; Lipenkov, V. Ya.; Hondoh, T. Diffusion of air molecules in polar ice sheets. In: *Physics of Ice Core Records;* T. Hondoh Ed.; Hokkaido University Press: Sapporo, Japan, 393−421.